Hot Wire Anemometer Turbulence Measurements in the wind Tunnel of LM Wind Power

Fischer, Andreas

Publication date:
2012

Document Version
Publisher's PDF, also known as Version of record

Hot Wire Anemometer Turbulence Measurements in the wind Tunnel of LM Wind Power

DTU Wind Energy Report E

Andreas Fischer
DTU Wind Energy Report E-0006(EN)
March 2012

DTU Wind Energy
Department of Wind Energy

Author: Andreas Fischer
Title: Hot Wire Anemometer Turbulence Measurements in the Wind Tunnel of LM Wind Power
Department: DTU Wind Energy

Abstract (max. 2000 char.): Flow measurements were carried out in the wind tunnel of LM Wind Power A/S with a Dantec Streamline CTA system to characterize the flow turbulence. Besides the free tunnel flow with empty test section we also investigated the tunnel flow when two grids with different mesh size were introduced downstream of the nozzle contraction. We used two different hot wire probes: a dual sensor miniature wire probe (Dantec 55P61) and a triple sensor fiber film probe (Dantec 55R91). The turbulence intensity measured with the dual sensor probe in the empty tunnel section was significantly lower than the one measured with the triple sensor probe. The turbulence intensity as well as the mean flow velocity downstream of the grids were not homogeneous in space. The grid with the finer mesh size created higher turbulence intensity. For both grids we found a functional form of the power spectral density of the velocity signal which is independent of the flow velocity and Reynolds number.

DTU Wind Energy Report
E-0006(EN)
March 2012

ISBN 978-87-92896-05-6

Contract no.:

Project no.:

Sponsorship:

Cover :

Pages: 30
Tables: 5
References: 7

Technical University of Denmark
Frederiksborgvej 399
4000 Roskilde
Denmark
Telephone +45 21327256
asfi@dtu.dk
www.vindenergi.dtu.dk

Contents

1 Introduction *5*

2 Methods *6*
2.1 The Wind Tunnel, Turbulence Grids and Hot Wire Mount *6*
2.2 The Hot Wire Equipment and Calibration *7*
2.3 Data Acquisition and Processing *10*

3 Measurement Results *12*
3.1 Flow Stability and Hot Wire Accuracy *12*
3.2 Turbulence Characteristics without Turbulence Grid *13*
3.3 Turbulence Statistics with Grid *15*
3.4 Turbulence Spectra with Grid *17*

4 Discussion and Conclusions *21*

A Sensor Data *24*

B Matlab Code *25*

C Correlation Function *29*

1 Introduction

The free stream turbulence characteristics have a significant influence on the boundary layer development of an aerofoil. The boundary layer development has in turn a large effect on the aerodynamic performance of the aerofoil. Therefore for the wind turbine industry the question arises how do the aerodynamic features of an aerofoil section found from wind tunnel tests compare to the performance of the aerofoil section installed on a MW wind turbine and subjected to atmospheric turbulence.
To answer this question the DAN-AERO MW Experiments [1] were conducted from 2007 to 2009. The experiments include test of wind turbine aerofoils in several wind tunnels as well as measurements on a full scale 3.6 MW wind turbine. One of the wind tunnels where the test took place was the wind tunnel of LM Wind Power A/S (LSWT). The aerofoils were tested in the free tunnel flow, but also in a turbulent flow generated by two turbulence grids with different mesh size introduced downstream of the contraction. The turbulence characteristics of the flow in the LSWT without turbulence grid were studied during its aerodynamic commissioning [2]. However, no conclusive study was conducted to reveal the characteristics of the grid induced turbulence.
This reports aims to characterize the grid induced turbulence and to reevaluate the free stream turbulence in the LSWT. Experiments conducted by scientists of Risø National Laboratory [3] showed a much higher turbulence intensity than the one found during the aerodynamic commissioning. The present study will rather confirm the results of Papenfuß[2] and show that difference was caused by the hot wire probe used in the measurements of [3].
In section 2 we introduce the wind tunnel and our measurement equipment. It is also outlined how the hot wire system was calibrated and how the data was processed. In section 3 we first present the results for the empty wind tunnel and compare the two hot wire sensors. In the second part we investigate turbulence characteristics downstream of the turbulence grids and give a function for the power spectral density of the velocity signal which is independent of the Reynolds number. The significance of our findings is pointed out in section 4.

2 Methods

2.1 The Wind Tunnel, Turbulence Grids and Hot Wire Mount

The Wind Tunnel of LM Wind Power A/S (LSWT)

The LSWT is a closed circuit wind tunnel with a closed test section, figure 1. The flow is driven by a 1MW fan. A flow speed of up 105m/s can be reached. The tunnel is equipped with a heat exchanger which can cool down the fluid to kept the temperature at a constant level. A good flow quality is achieved with aerodynamically treated corner vanes, a honeycomb structure, 3 screens and a nozzle with a contraction ratio of 10 to 1. The test section is 7m long and has

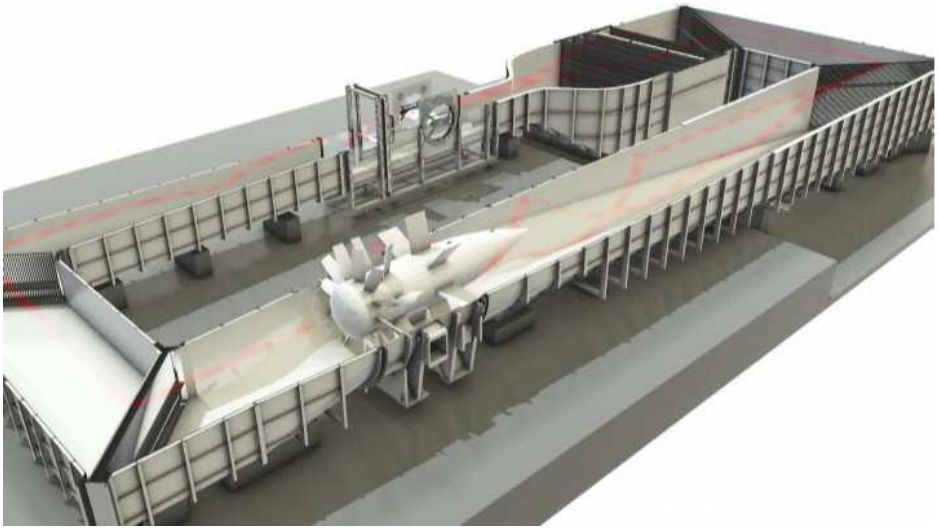

Figure 1. The wind tunnel of LM Wind Power A/S (LSWT) (from [4])

a cross section of 1.35m of width and 2.7m of height. The aerofoils tested in the wind tunnel span the width and are mounted between two turn tables with the trailing edge 5.2 m downstream of the end of the contraction. The typical chord length is 0.9m.

The Turbulence Grids and the Hot Wire Mount

Two grids of different mesh size were used. The first one denoted by fine grid (FG) has a mesh size of 100mm x 100mm. The second one denoted by coarse grid (CG) has a mesh size 200mm x 200mm. They are made of aluminum plates with a width (streamwise length scale when mounted in the LSWT) of 35mm and a thickness of 3mm. The turbulence grids were placed 0.4 m downstream of the contraction.

The hot wire sensors were mounted on a traverse system in the test section, figure 2(b). The traverse system was originally designed for mapping the boundary layer at the trailing edge of an aerofoil section. The hot wire sensor tip was placed at approx. 5.2m downstream of the contraction (the position of the trailing edge of the normally tested airfoils). This corresponds to the position of the trailing edge of a aerofoil section when tested in the tunnel. The hot wire sensor was approximately centered in the cross section. Figure 3 shows the orientation of the flow components measured by hot wire sensor in the test section of the LSWT.

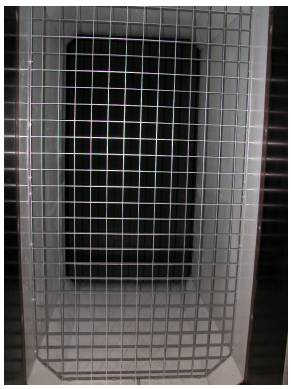

(a) The fine grid

(b) The hot wire sensor mount

Figure 2. The wind tunnel setup

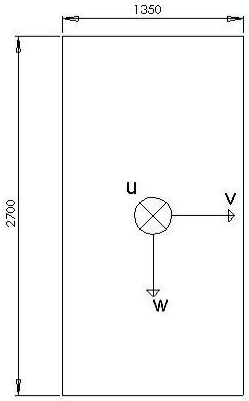

Figure 3. Cross sectional view of the test section with orientation of the probe velocity components, u pointing in the paper plane

Note that the XW probe only measures the u and w component. The hot wire traverse systems allows a change of position in vertical direction of 83.8mm. The position denoted by 0mm is the lowest vertical position, approximately the middle of the test section. The position relative to the turbulence grid was not measured.

2.2 The Hot Wire Equipment and Calibration

Streamline CTA module signal conditioner, A/D board NI e series, miniature X wire probe (Dantec 55P61)(abbreviated as XW in the following), triple wire fiber film probe (Dantec 55R91)(abbreviated as 3D in the following), Dantec temperature probe.
Both hot wire sensors were operated with overheat ratio $a = 0.8$ and the reference temperature was set to 19^oC. To compensate for temperature fluctuations of the tunnel flow, a temperature correction according to [5] was applied. A temperature load factor of $m = 0.2$ was chosen. We used this setting throughout the whole measurement campaign.
The velocity calculated from the difference of the pressure measured at nozzle inlet and nozzle outlet with LM's measurement system was the reference for the calibration. The hot wire voltage output was measured and averaged with the StreamWare software. The sampling frequency was 1 kHz and 32768 samples per calibration velocity were taken. For the temperature correction the test section

(static) temperature measured by LM's system was used. The temperature corrected voltage output of the XW probe over the flow velocity is illustrated in figure 4. For the subsequent transformation of hot wire voltage output into velocity two

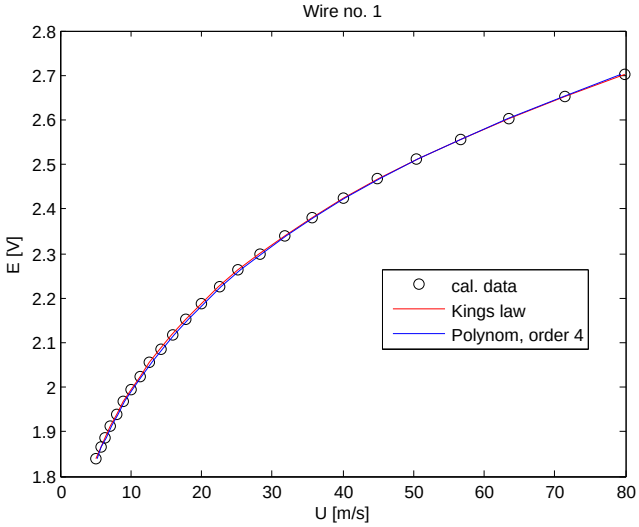

(a) XW probe wire 1

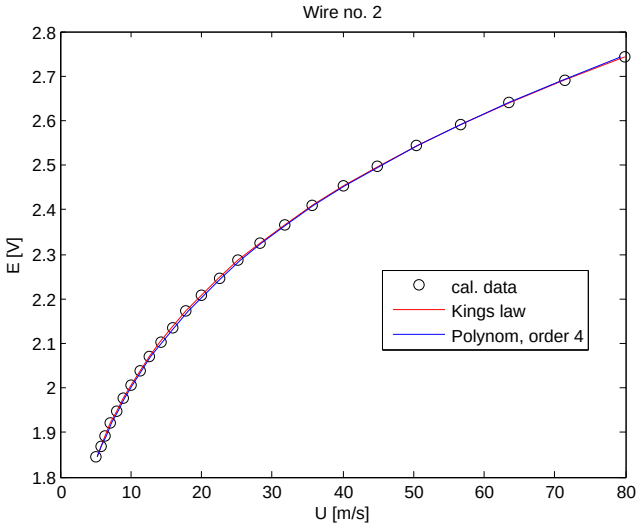

(b) XW probe wire 2

Figure 4. Calibration Data for the XW wire probe [Note: the voltage is temperature corrected]

different functions were considered: king's law (see reference [6] for details) and a polynomial of order 4. King's law is appropriate if the velocity exceeds the highest calibration during an experiment, because a polynomial may oscillate when the calibration range is exceeded. However, within the calibration range, the polynomial is most often more accurate [7].
The error induced by the velocity/voltage conversion function was calculated with equation 1.

$$\varepsilon = \frac{U_{comp} - U_{cal}}{U_{cal}} \tag{1}$$

U_{comp} denotes the velocity computed from the hot wire voltage with the respective conversion function and U_{cal} stands for the calibration reference velocity measured with LM's system. The data conversion error for the XW probe is smaller when

using king's law, figure 5. I chose to take King's law for the voltage/velocity

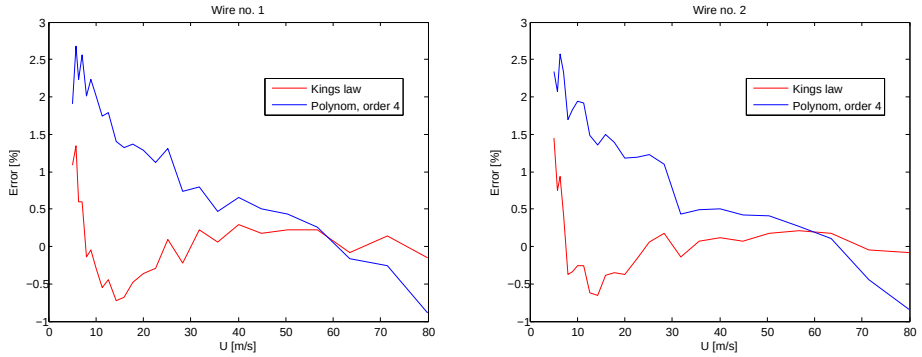

(a) XW probe wire 1 (b) XW probe wire 2

Figure 5. Data Conversion Error for the XW probe

conversion of the XW probe for all data presented in this report.
The data conversion error of the 3D probe over the flow velocity is illustrated in figure 6. Note that the error is much bigger than the data conversion error for the

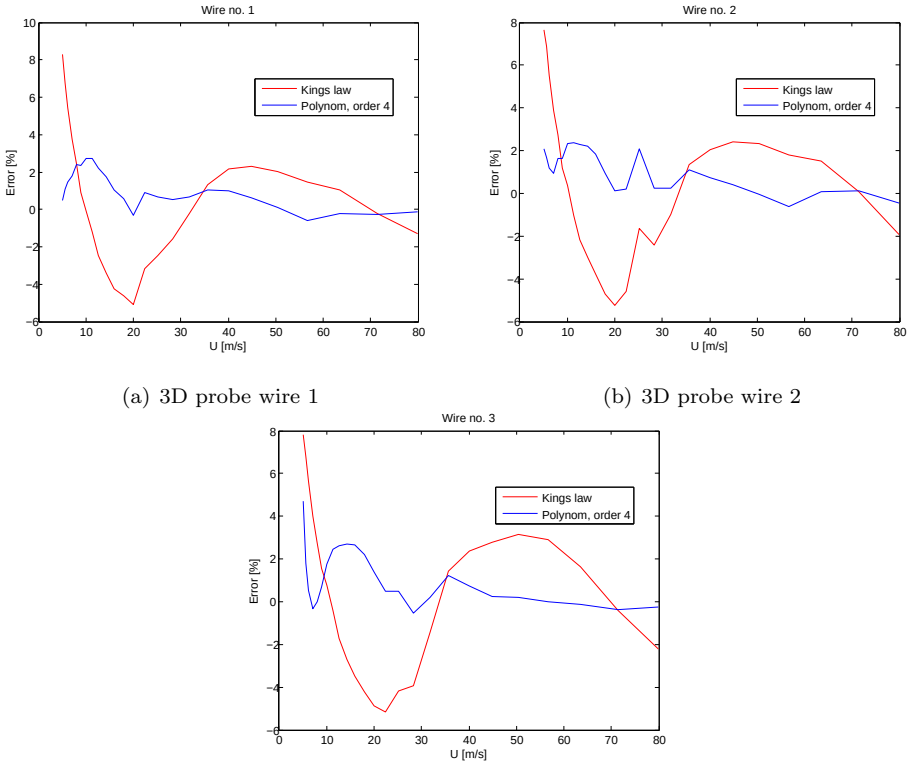

(a) 3D probe wire 1 (b) 3D probe wire 2

(c) 3D probe wire 3

Figure 6. Data Conversion Error for the 3D probe

XW probe. King's law gives a very poor approximation of the voltage/velocity function of the 3D probe. A possible explanation might be that the wires of the 3D probe (fiber film, 70μm diameter) are of different material and diameter than the wires of the XW probe (tungsten, 5μm diameter) and don't follow the same

law. Consequently, the 4th order polynomial was used for the voltage/velocity conversion of the 3D probe.

2.3 Data Acquisition and Processing

The StreamWare software was used for the data acquisition during the experiment. The sampling frequency was set to 25 kHz and a number of samples of $20097152 = 2^{21}$ was collected during each event. It yields a sampling time of approximately 83.9s. A low pass filter with a cut-off frequency of 10 kHz was applied to avoid aliasing. For the temperature correction the temperature measured by the Dantec temperature probe was used.
An overview of the measurements and the respective conditions is given in table 1. The hot wire probe was kept fixed at z-position 0mm for measurements without

Meas. ID	LM ID no.	grid	hot wire	flow speed [m/s]	temp. [^oC]
1	181843	none	XW	26.96	18.4
2	181844	none	XW	49.95	19.3
3	181845	none	XW	66.96	19.7
4	181840	none	3D	26.95	17.5
5	181841	none	3D	49.99	18.7
6	181842	none	3D	67.00	19.2
7	181846	CG	XW	26.99	18.5
8	181848	CG	XW	50.03	19.0
9	181850	CG	XW	67.01	19.2
10	181851	CG	3D	27.01	18.6
11	181853	CG	3D	50.03	18.9
12	181855	CG	3D	67.01	19.7
13	181869	FG	XW	27.02	18.5
14	no data	FG	XW	(50)	-
15	no data	FG	XW	(67)	-
16	181857, 59	FG	3D	27.00	18.6
17	181861, 63, 65	FG	3D	50.00	19.1
18	181867	FG	3D	67.00	20.0

Table 1. Measurement overview (flow speed and temperature from LM sensor)

turbulence grid. With the XW probe 2 subsequent measurements were taken, with the 3D probe 3 subsequent measurements. The XW probe was placed at 6 positions for the measurements with turbulence grids, linearly distributed from 0mm to 83.8mm. The 3D probe was placed at 3 positions for the measurements with turbulence grids, z=0mm, 50.28mm and 83.8mm.
Bertagnolio [5] found some problems when using the StreamWare software to compute the hot wire velocities. Hence, I used an inhouse MATLAB routine to convert voltage into velocity. The source code can be found in Appendix B. I followed the equations given on page 30 of [7] to perform the conversion. Note that the second set of equations given by Dantec [7] is only an approximation to the correct expression. The term $k_1^2 k_2^2$ was ignored when compared to 1. The

correct expression is given by equation 2.

$$
\begin{aligned}
U_1 &= \frac{\sqrt{2}}{2}\sqrt{\frac{1}{k_1^2k_2^2-1}\left[(1+k_1^2)k_2^2U_{cal1}^2-(1+k_2^2)U_{cal2}^2\right]} \\
U_2 &= \frac{\sqrt{2}}{2}\sqrt{\frac{1}{k_1^2k_2^2-1}\left[-(1+k_1^2)U_{cal1}^2+(1+k_2^2)k_1^2U_{cal2}^2\right]}
\end{aligned} \tag{2}
$$

I used equation 2 instead of the relation given by Dantec [7] in the MATLAB routine.
The turbulence intensity for the XW probe was not calculated by the standard definition (equation 3), because only the u- and w-component were measured. Therefore the expression given by equation 4 was used.

$$
T_{i,3D} = \sqrt{\frac{\frac{1}{3}(\langle u^2\rangle+\langle v^2\rangle+\langle w^2\rangle)}{\langle U\rangle^2+\langle V\rangle^2+\langle W\rangle^2}} \tag{3}
$$

$$
T_{i,XW} = \sqrt{\frac{\frac{1}{2}(\langle u^2\rangle+\langle w^2\rangle)}{\langle U\rangle^2+\langle W\rangle^2}} \tag{4}
$$

The lower case letters indicate that the mean value is subtracted from the time series, i.e. $u = U - \langle U\rangle$.
The power spectral density (PSD) of the velocity components was calculated with the MATLAB algorithm *pwelch*. The time series was divided into 256 segments of 8192 samples. This yields a frequency resolution of 3.05 Hz.
The spectra taken for different flow conditions or turbulence grids can be better compared when plotted as function of the non-dimensional Strouhal number instead of the frequency. The Strouhal number is defined in expression 4.

$$
St = \frac{fL}{\overline{V}} \tag{5}
$$

f denotes the frequency, L a reference length scale and $\overline{V}$ the mean flow speed. The relation between the PSD as function of the frequency and the PSD as function of the Strouhal number follows directly from eq. 5. It is given by eq. 6.

$$
PSD(St) = \frac{\overline{V}}{L}PSD(f) \tag{6}
$$

3 Measurement Results

3.1 Flow Stability and Hot Wire Accuracy

One measurement event as listed in table 1 took up to 15 minutes. Therefore I first checked how stable the flow conditions provided by the LSWT were over such a period of time. A direct comparison of velocity time series measured by LM and hot wire sensors was not possible (due to synchronization problems). Figure 7 shows time series of velocity measurements with LM sensors for some of the longest consecutive measurements made in this campaign. None of the 3 examples

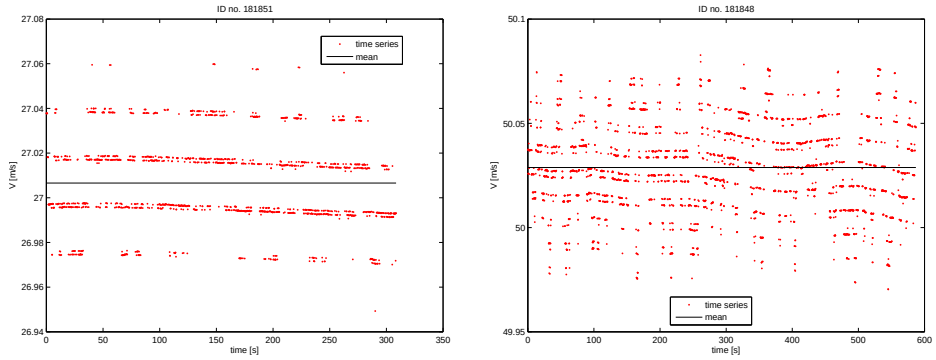

(a) Measurement ID 10 (See table 1)

(b) Measurement ID 8 (See table 1)

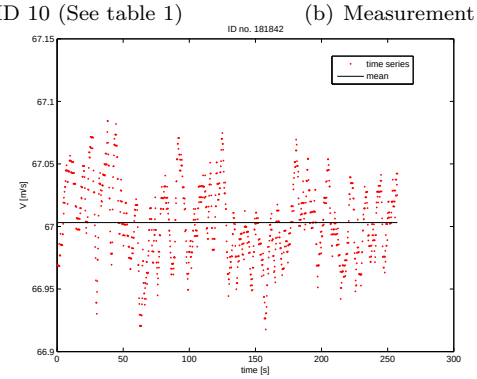

(c) Measurement ID 6 (See table 1)

Figure 7. Velocity time series measured with LM reference sensor

shows a drift in mean velocity. The low frequency fluctuations detected by LM's measurement system are less than ±0.1m/s about the mean.
To check the accuracy of the hot wire calibration, the mean velocities measured with the hot wire sensors and with LM's system are compared in table 2 for all measurements without turbulence grid. In general, the mean velocity measured with the XW probe agrees better with the reference velocity than the mean velocity measured with the 3D probe. The 3D probe tends to overestimate velocities if the mean velocity is low and underestimate, if the mean velocity is high. The flow speed drift in the measurement with the 3D probe at about 67m/s is not detected by LM's sensor (figure 7(c)).

3D probe	V[m/s](error[%]) Measurement no.		
V LM sensor [m/s]	1	2	3
26.95	27.28(1.23)	27.32(1.37)	27.35(1.48)
49.99	49.91(−0.17)	49.94(−0.11)	49.95(−0.09)
67.00	66.80(−0.30)	66.66(−0.51)	66.45(−0.82)

XW probe	V[m/s](error[%]) Measurement no.	
V LM sensor [m/s]	1	2
26.96	27.03(0.25)	26.96(−0.00)
49.95	49.94(−0.02)	49.92(−0.07)
66.96	67.24(0.42)	67.19(0.36)

Table 2. Velocities from Hot Wire Probes compared to Velocity from Contraction Pressure Difference

3.2 Turbulence Characteristics without Turbulence Grid

The turbulence intensity measured with both sensors vs. the flow speed is illustrated in figure 8. The turbulence intensity computed from the measurements

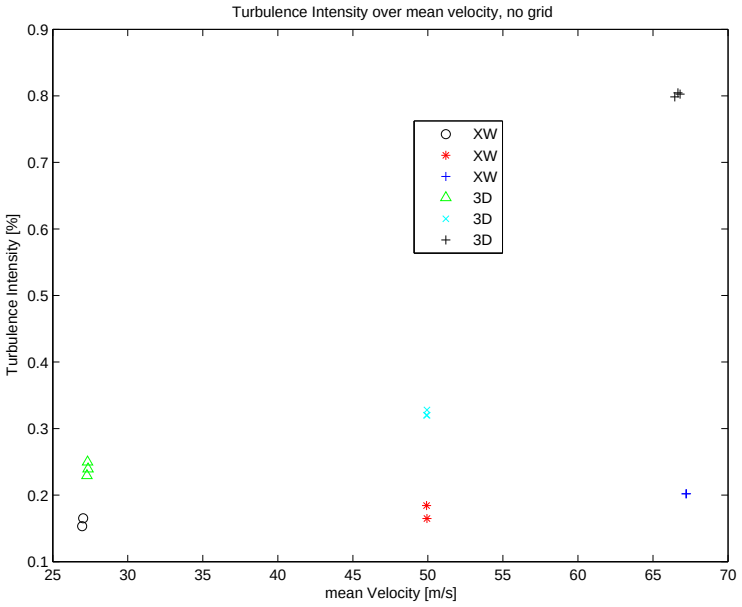

Figure 8. Turbulence intensity over flow speed

with the XW probe are much lower than the ones computed from the measurements with the 3D probe. The XW probe turbulence intensities increase slightly with flow speed. The 3D probe turbulence intensities increase strongly with flow speed. Especially from 50m/s to 67m/s a very strong change is observed. If the 3D probe measured the right turbulence intensity, the variance of the v-component (not measured with the XW probe) must be substantially higher than the u- and w-component. However, this is not generally supported by the analysis of the component wise variance, table 3. Two out of three measurements obtain a much greater variance of the v-component at a wind tunnel flow speed of 27m/s. But at 50m/s and 60m/s the variance of the v- and w-component is of the same order of magnitude and they are much greater than the variance of the u-component (3D probe). The XW probe reveals a completely different trend: the variance of

event no.	type	V [m/s]	$< u^2 >$ [m^2/s^2]	$< v^2 >$ [m^2/s^2]	$< w^2 >$ [m^2/s^2]
1	3D	27.28	$3.09 \cdot 10^{-3}$	$7.19 \cdot 10^{-3}$	$1.47 \cdot 10^{-3}$
2	3D	27.32	$6.15 \cdot 10^{-3}$	$6.41 \cdot 10^{-3}$	$1.42 \cdot 10^{-3}$
3	3D	27.35	$3.13 \cdot 10^{-3}$	$8.19 \cdot 10^{-3}$	$1.55 \cdot 10^{-3}$
1	XW	27.03	$3.54 \cdot 10^{-3}$	-	$0.45 \cdot 10^{-3}$
2	XW	26.96	$2.97 \cdot 10^{-3}$	-	$0.44 \cdot 10^{-3}$
1	3D	49.91	$0.94 \cdot 10^{-2}$	$3.47 \cdot 10^{-2}$	$3.25 \cdot 10^{-2}$
2	3D	49.94	$0.92 \cdot 10^{-2}$	$3.62 \cdot 10^{-2}$	$3.51 \cdot 10^{-2}$
3	3D	49.95	$0.89 \cdot 10^{-2}$	$3.44 \cdot 10^{-2}$	$3.32 \cdot 10^{-2}$
1	XW	49.94	$1.06 \cdot 10^{-2}$	-	$0.29 \cdot 10^{-2}$
2	XW	49.92	$1.39 \cdot 10^{-2}$	-	$0.30 \cdot 10^{-2}$
1	3D	66.80	$1.04 \cdot 10^{-1}$	$3.80 \cdot 10^{-1}$	$3.78 \cdot 10^{-1}$
2	3D	66.66	$1.09 \cdot 10^{-1}$	$3.77 \cdot 10^{-1}$	$3.77 \cdot 10^{-1}$
3	3D	66.45	$0.99 \cdot 10^{-1}$	$3.72 \cdot 10^{-1}$	$3.74 \cdot 10^{-1}$
1	XW	67.24	$3.25 \cdot 10^{-2}$	-	$0.44 \cdot 10^{-2}$
2	XW	67.19	$3.23 \cdot 10^{-2}$	-	$0.45 \cdot 10^{-2}$

Table 3. The variances of the velocity components

the u-component is greater than the variance of the w-component over the whole velocity range. The high turbulence intensities measured with the 3D probe lead to the conclusion that the probe might generate turbulence by itself which is dependent on the flow speed (Reynolds number). The wires of the 3D probe are 14 times thicker than the wires of the XW probe and the geometry of the 3D probe is much more complex. The power spectral density (PSD) of the velocity components measured with the 3D probe at wind tunnel flow speed 67m/s (figure 9) shows the characteristics of a turbulent flow while the PSD of the velocity components measured with the XW probe shows rather the characteristics of a random noise signal and has a lower overall level. If the high turbulence level measured with the

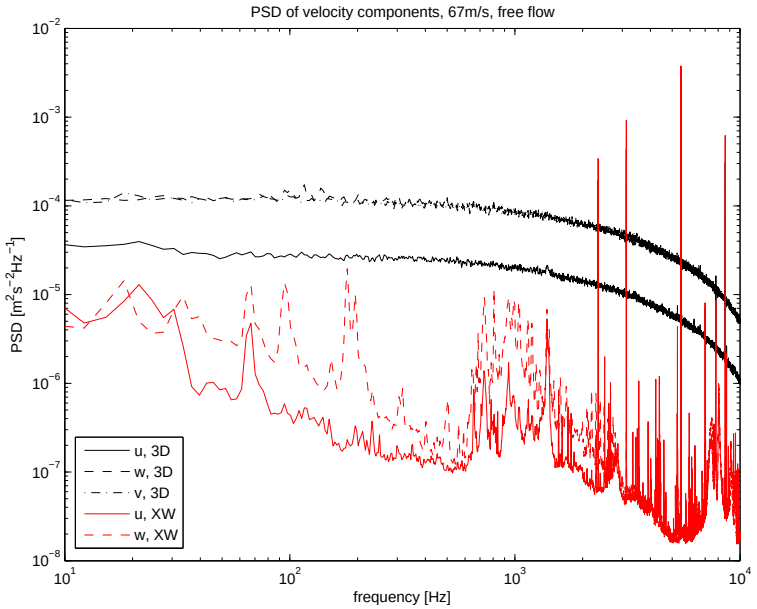

Figure 9. Power Spectral Density of Velocity Components at Flow Speed 67m/s, no turbulence grid

3D probe at 67m/s was generated by the wind tunnel flow, one would also detect

it in the PSD with the XW probe.
The shape of the PSD of the XW probe suggests that the measured fluctuations are not generated by wind tunnel turbulence, but either by the electric noise level of the data acquisition system and hot wire power supply or by vibrations induced by the stepper motor (when the stepper was supplied with current a vibration could actually be felt, but not quantified). This could explain why the turbulence intensities measured with the XW probe are almost a factor of 2 higher than the ones measured during the commissioning [2].

3.3 Turbulence Statistics with Grid

The turbulence intensity measured with both sensors at different flow velocities with the fine grid inserted is not homogeneous in space, figure 10. The total travers-

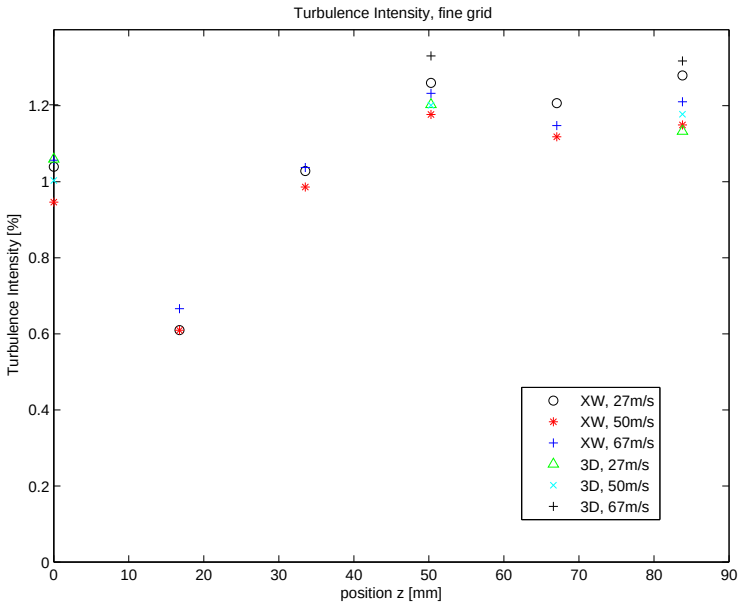

Figure 10. Turbulence Intensity generated by the Fine Grid

ing distance (83.8mm) does not cover one mesh size (100mm). The turbulence intensity varies from minimum to maximum by a factor of 2. It is only weakly dependent on flow speed. Only the measurement with the 3D probe at flow speed 67m/s shows a significantly higher level than the other measurements. Though, this might be caused by the 3D probe itself as discussed above.
The mean velocity varies in space as well, figure 11. The magnitude of the variations of the mean velocity is higher than the measurement uncertainty and the flow speed variations in the tunnel. This flow inhomogeneity must be generated by the turbulence grid.
One can draw conclusions about the position of the turbulence grid relative to the hot wire probe by the pattern of the flow inhomogeneity. I expect the middle of the mesh at the height position of the minimum of the turbulence intensity and maximum of mean flow speed, i.e. z=16.76mm. The frame of the mesh is at the position of the minimum of the flow speed, i.e. z=67.04mm.
The turbulence intensity level generated by the coarse grid is lower than the level generated by the fine grid, figure 12. The values measured with the 3D probe at flow speed 67m/s are much higher than all other measurements. They are of the same magnitude as the turbulence intensity measured with the 3D probe at flow

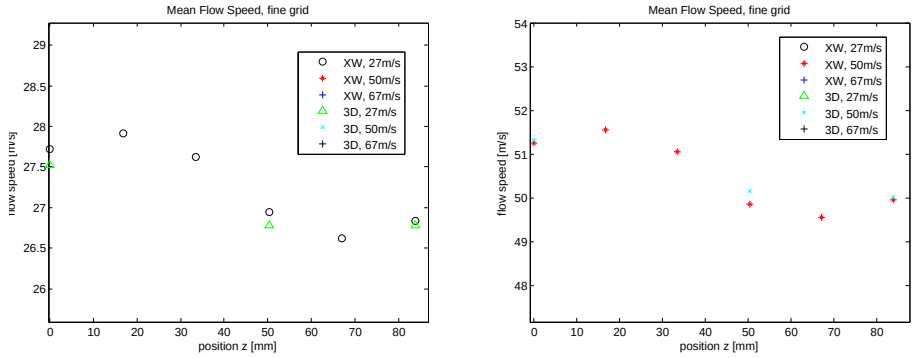

(a) wind tunnel flow speed 27m/s (b) wind tunnel flow speed 50m/s

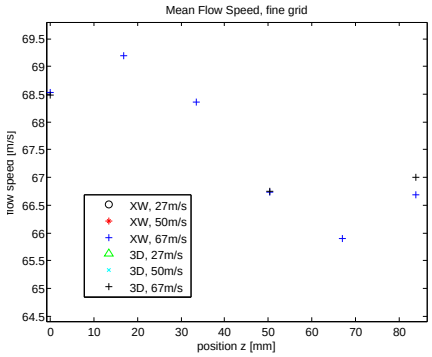

(c) wind tunnel flow speed 67m/s

Figure 11. Mean Flow Speed vs. Position, fine grid

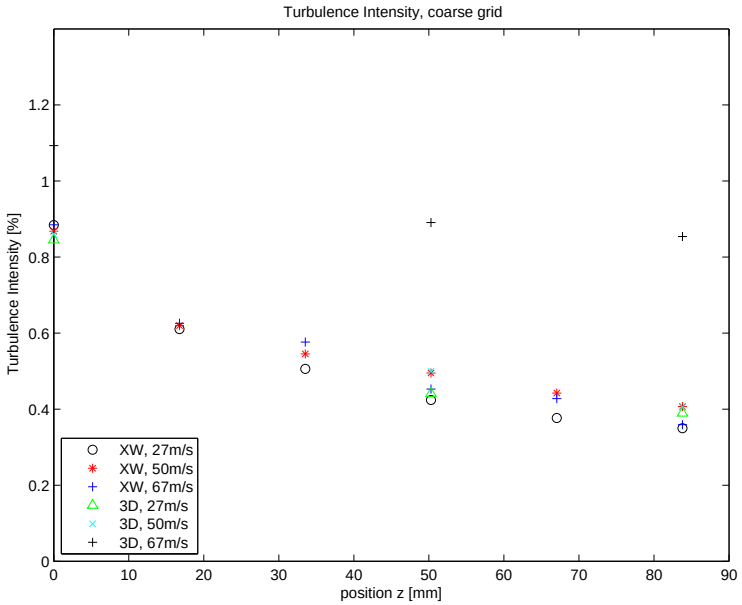

Figure 12. Turbulence Intensity generated by the Coarse Grid

speed 67m/s without turbulence grid. It indicates that the grid generated turbulence is superimposed with self generated turbulence in this case and the levels are biased high. If we ignore these outliers, the turbulence intensity is found independent of flow speed. Again, the turbulence field is not homogeneous in space.

It decreases monotonously from position z=0mm to 83.8mm, but the traversing distance does not cover half a mesh size.
The mean flow speed vs. position is plotted in figure 13. The variations of the mean

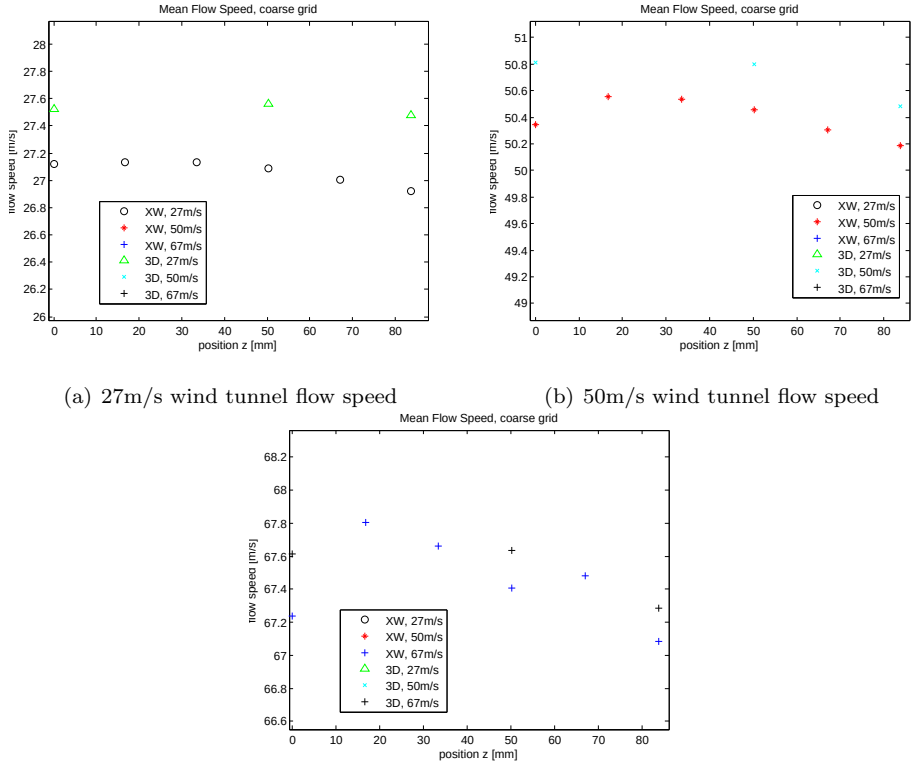

(a) 27m/s wind tunnel flow speed

(b) 50m/s wind tunnel flow speed

(c) 67m/s wind tunnel flow speed

Figure 13. Mean Flow Speed vs. Position, coarse grid

flow speed seem to be systematic, but on the other hand the variations about the mean are in the worst case ±0.5%. This is roughly equal to the uncertainty of the mean flow measurement.

3.4 Turbulence Spectra with Grid

The PSD over the Strouhal number is shown in figure 14 for the two different grids and a flow speed of 50m/s . The reference length for the Strouhal number is the mesh size (100mm for FG and 200mm for CG). The PSD(St) is normalized by the square of the mean velocity to make it non-dimensional. It will be shown in the following analysis that this is the correct scaling law for the level of the PSD. The measurement position was also normalized by the mesh size. However, the position of the mesh frame relative to the probe position is not known and it is most probably different for the two grids. Figure 14 shows that scaling the frequency and PSD with the mesh size does not collapse the data. The velocity scaling does not play a role in this comparison, because both measurements were made with the same flow speed. Hence, the mesh size is not a proper length scale for the grid generated turbulence. Figure 15 displays a similar plot as figure 14, but the reference length for the Strouhal number is the same for both grids (arbitrary chosen as L=1m). The measurement position is normalized with the mesh size. The data does not collapse either if the same length scale is used for both grids. It is not sure if a length scale exists which collapses the data. In the following the

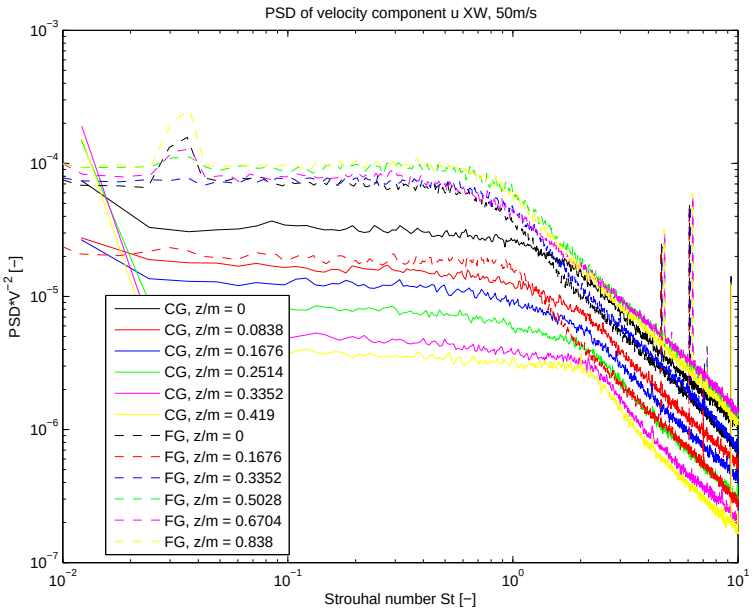

(a) u component

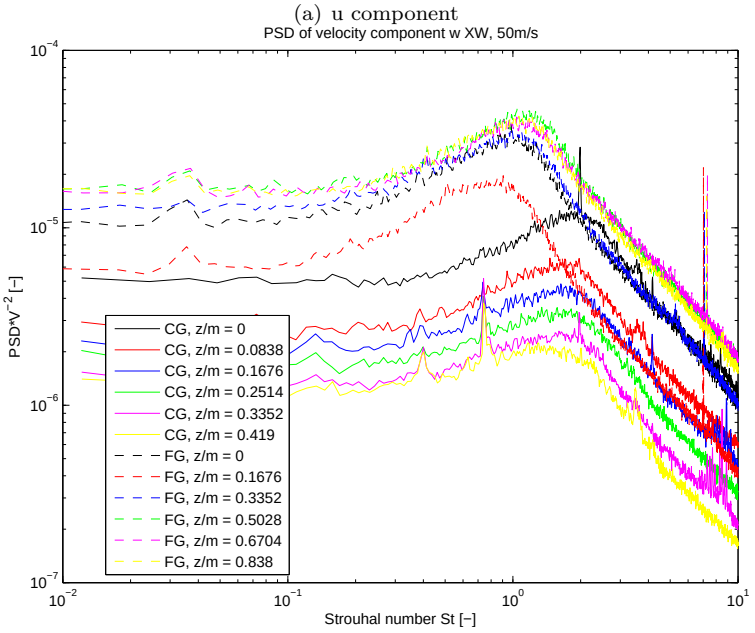

(b) w component

Figure 14. normalized PSD over Strouhal number (reference length = mesh size) for CG and FG, Flow Speed 50m/s

somewhat arbitrary length scale of 1m is used.
Figure 16 depicts the PSD vs. the Strouhal number for the two grids and different flow velocities at two arbitrary chosen measurement positions. The data collapses if the PSD is scaled with the square of the mean flow speed. The good agreement of the spectral shape suggests that the physical mechanisms generating the turbulence are independent of the flow speed (Reynolds number) in the range we investigated. The scaling of the level of the PSD with the mean flow velocity to a power of 2 is equivalent with a constant turbulence intensity over mean flow velocity. We found this earlier.

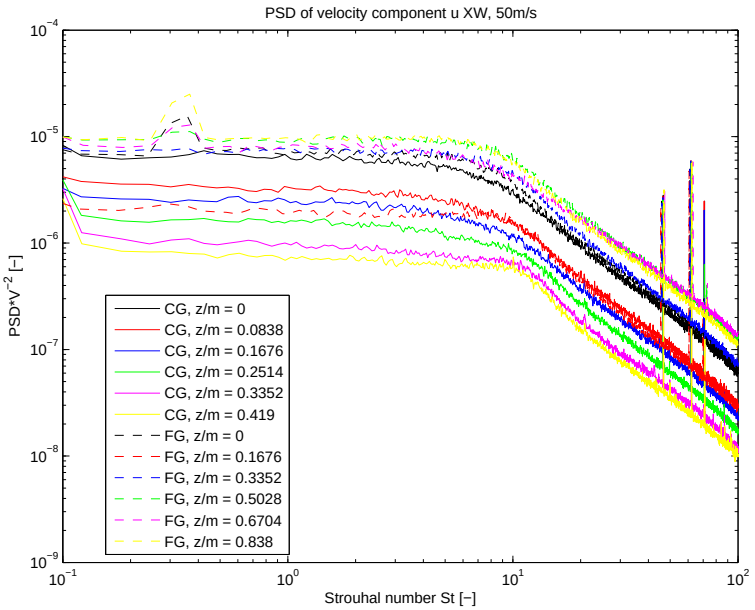

(a) u component

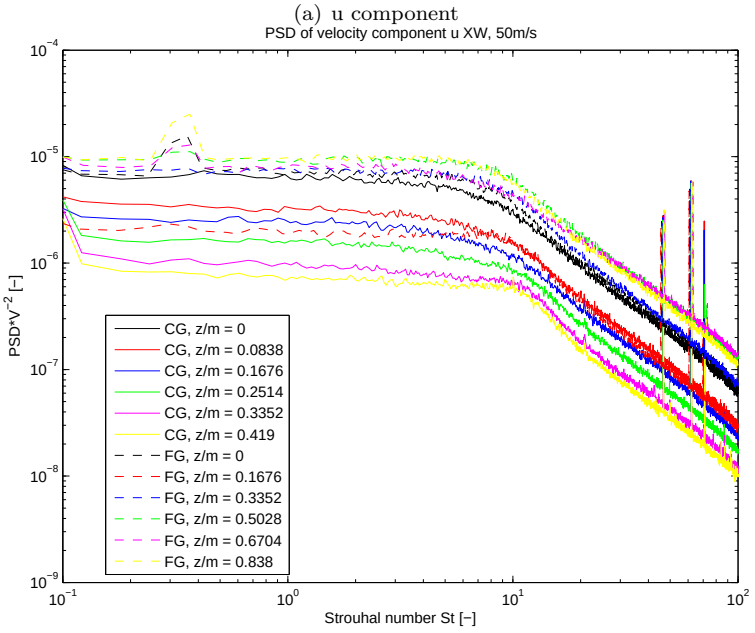

(b) w component

Figure 15. normalized PSD over Strouhal number (reference length = 1m) for CG and FG, Flow Speed 50m/s

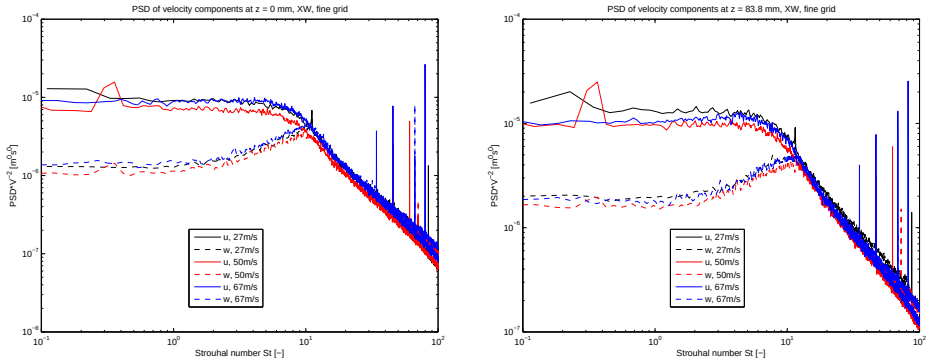

(a) position z=0mm, FG

(b) position z=83.8mm, FG

(c) position z=0mm, CG

(d) position z=83.8mm, CG

Figure 16. normalized PSD over Strouhal number (reference length = 1m) for FG and CG, varying Flow Speed

4 Discussion and Conclusions

We performed flow measurements in the wind tunnel of LM Wind Power A/S (LSWT). The aim of the measurements was to characterize the properties of the turbulence in the test section of the tunnel for 3 different configurations: the empty tunnel and the tunnel with two different grids inserted after the nozzle contraction. We used a dual sensor miniature wire probe (Dantec 55P61)(XW) and a triple sensor fiber film probe (Dantec 55R91)(3D) to perform two independent measurements for each configuration.

The measurements with the 3D probe revealed significantly higher turbulence intensities than the measurements with the XW probe, especially at high flow velocities. The analysis of the power spectra density (PSD) of the velocity signal suggests that the 3D probe generates turbulence by itself. The diameter of its wires is 14 times larger than the diameter of the wires of the XW probe and its geometry is much more complex. Probe generated turbulence would also explain the fact that the turbulence intensities measured by Risø scientists [3] (using a 3D type probe) are much higher than the turbulence intensity measured by Papenfuß[2] (using a XW type probe). The turbulence intensities measured with the XW probe in the present campaign are between 1.5 and 2 times higher than the one measured by Papenfuß[2]. The analysis of the PSD of velocity signal shows some noise contamination for the measurements in the empty tunnel configuration, because we did not use a high pass filter and gain when measuring very low turbulence intensities. Therefore the results of Papenfuß[2] are considered to be the most reliable. But on the other hand, it is still not clarified if the turbulence intensity does not increase when an airfoil is inserted, because the turbulence generated by the boundary layer of the airfoil can circulate in the tunnel.

Investigating the characteristics of the grid generated turbulence, we focused on the results of the measurements with the XW probe, because the XW probe proved to be more reliable than the 3D probe. The mean flow velocity and turbulence intensity downstream of the fine grid (FG) was inhomogeneous in space. The traversing distance covered only 84% of one mesh size, but the flow inhomogenity was sufficiently described by the measurements. The mean flow velocity downstream of the coarse grid (CG) shows a monotonous decrease, but the absolute difference between maximum and minimum was so small that it was not possible to make a clear statement about mean flow homogenity with the present measurement accuracy. The turbulence intensity was inhomogeneous. The traversing distance (42% of one mesh size) was not big enough to give a full picture of the flow inhomogenity. The turbulence intensity was independent of the flow speed (Reynolds number) for both grids. The FG generated a higher turbulence intensity than the CG.

The PSD of the velocity signal was calculated in dependence of the Strouhal number and normalized by the square of the mean velocity. The normalized PSD was independent of the mean flow speed. The non-dimensionalized form of the PSD is very well suited for modeling the grid generated turbulence. However, it was not possible to find the right length scale to make the results independent of the characteristics of the turbulence grid. It is not sure if this is possible at all. An investigation of the integral length scale of the turbulence at different positions might give a clue. The integral length scale can be evaluated from the correlation function given in Appendix C.

For future experiments, I recommend to use a XW type probe instead of a 3D type. All 3 velocity components can be measured with the XW probe by doing 2 separate measurements and rotating the probe around its axis by 90^o. To fully characterize the flow downstream of the CG, a distance of 200mm should be tra-

versed. The signal of the hot wire probe has to be conditioned (high pass filter and gain) to measure the turbulence intensity in the empty tunnel section correctly.

References

[1] H.A. Madsen, C. Bak, U.S. Paulsen, M. Gaunaa, P. Fuglsang, J. Romblad, N.A. Olesen, P. Enevoldsen, J. Laursen, and L. Jensen. The DAN-AERO MW Experiments: Final report. Tech. Rep. Risø-R-1726(EN), Risø-DTU, Roskilde, Denmark, September 2010.

[2] H. D. Papenfuß. Aerodynamic Commissioning of the New Wind Tunnel at LM Glasfiber A/S (Lunderskov); Private Communication. Property of LM Glasfiber, June 2006.

[3] F. Bertagnolio. NACA0015 Measurements in LM Wind Tunnel and Turbulence Generated Noise. Tech. Rep. Risø-R-1657(EN), Risø-DTU, Roskilde, Denmark, November 2008.

[4] P. Bæk. Experimental Detection of Laminar to Turbulent Boundary Layer Transition on Airfoils in an Industrial Wind Tunnel Facility. Master's thesis, The Technical University of Denmark DTU, September 2008.

[5] F. Bertagnolio. Boundary Layer Measurements of the NACA0015 and Implications for Noise Modeling. Tech. Rep. Risø-R-1761(EN), Risø-DTU, Roskilde, Denmark, January 2011.

[6] H.H. Bruun. *Hot-Wire Anemometry: Principles and Signal Analysis.* Oxford University Press, 1995.

[7] F. E. Jørgensen. How to Measure Turbulence with Hot-Wire Anemometer - A Practical Guide. Available at: http://www.dantecdynamics.com/Admin/Public, 2004.

A Sensor Data

The sensor data relevant for the voltage to velocity conversion is given in table 4 and 5.

	1	2
R_{20} [Ω]	3.47	3.45
R_L [Ω]	0.5	0.5
α_{20}[%]	0.36	0.36

Table 4. Data of Probe Type Dantec 55P61

	1	2	3
R_{20} [Ω]	5.49	5.61	5.96
R_L [Ω]	0.5	0.5	0.5
α_{20}[%]	0.42	0.43	0.44

Table 5. Data of Probe Type Dantec 55R91

B Matlab Code

The script *CreateCalData3.m* computes the calibration functions and the error linked to the calibration function. The calibration functions are saved in Matlab binary format.

```
clear all;close all;clc;
% open hot wire data file
[file,path]=uigetfile('*.*','Select hot wire calibration data file');
nHW=input('Enter number of wires of HW sensor (as integer) : ');
dout=defaultread(strcat(path,file),1,3+3*nHW,1:3+nHW);
Ucal=dout(1,:)';Ecal=dout(2:nHW+1,:)';Tcal=dout(2+nHW,:)';Pcal=dout(3+nHW,:)';
%gather information
Tref=input('Enter reference temperature[C] : ');
R=input('Enter overheat ratio : ');
Tcr20=input('Enter wire temp. coeff. of resistance at 20C (as vector): ');
m=input('Enter temperature load factor : ');
Tw=Tref*ones(size(Tcr20))+(R*ones(size(Tcr20)))./(Tcr20./(ones(size(Tcr20))+Tcr20*(Tref-20)));
np=input('Enter order of calibration polynom as integer : ');
% apply temperature correction
ilt=find(Tcal<Tref);iht=find(Tcal>=Tref);
tcex=zeros(size(Tcal));
tcex(iht)=(1+m)/2;tcex(ilt)=(1-m)/2;
Ecalc=zeros(size(Ecal));
for nw=1:nHW
    Ecalc(:,nw)=Ecal(:,nw).*((Tw(nw)-Tref)./(Tw(nw)*ones(size(Tcal))-Tcal)).^tcex;
    % create calibration polynom of order np
    CalPol(:,nw)=polyfit(Ecalc(:,nw),Ucal,np);
    % create calibration curve according to King's law
    resi(nw)=1000;
    for nexp=0.3:0.001:0.7
        A=polyfit(Ucal.^nexp,Ecalc(:,nw).^2,1);
        res=sum((Ucal-((Ecalc(:,nw).^2-A(2))/A(1)).^(1/nexp)).^2)/length(Ucal);
        if res<resi(nw)
           CalCo(:,nw)=A;ne(nw)=nexp;resi(nw)=res;
        end
    end
    Ucp=zeros(size(Ucal));
    for nnp=1:(np+1)
        Ucp=Ucp+CalPol(nnp,nw)*Ecal(:,nw).^(np-nnp+1);
    end
figure(2*nw-1)
plot(Ucal,Ecalc(:,nw),'ko',((Ecalc(:,nw).^2-CalCo(2,nw))/CalCo(1,nw)).^(1/ne(nw)),...
Ecalc(:,nw),'r',Ucp,Ecalc(:,nw),'b')
xlabel('U [m/s]');ylabel('E [V]');
legend('cal. data','Kings law',['Polynom, order ' num2str(np)],'Location','Best');
title(['Wire no. ' num2str(nw)]);
figure(2*nw)
plot(Ucal,(((Ecalc(:,nw).^2-CalCo(2,nw))/CalCo(1,nw)).^(1/ne(nw))-Ucal)./Ucal*100,'r',...
Ucal,(Ucp-Ucal)./Ucal*100,'b')
xlabel('U [m/s]');ylabel('Error [%]');
legend('Kings law',['Polynom, order ' num2str(np)],'Location','Best');
title(['Wire no. ' num2str(nw)]);
```

```
end
savecal=input('Do you want to save the calibration data? (1=yes, 0=no) : ');
if savecal
    savename=input('Enter name for saving calibration data: ','s');
    save(strcat(savename,'.mat'),'Ecal','Ecalc','Ucal','Tcal','Pcal','Tref',...
     'R','Tcr20','m','CalCo','ne','CalPol','np');
end
```

The script *PostProHWdata.m* computes the velocity from the hot wire voltage as well as the PSD and the first and second order statistical moments of teh velocity series. It uses the calibration data generated by *CreateCalData3.m* and the functions *Ucal2Vprobe.m*, *rotHWvel.m* and *TurbInt.m*.

```
clear all;close all;clc;
symbols={'k','b','r'};
% open hot wire data file
[file,path]=uigetfile('*.*','Select hot wire data file');
nchannel=input('Enter number of channels in hot wire data file : ');
nblock=input('Enter number of data blocks in hot wire data file : ');
nchT=input('Enter number of temperature sensor channel : ');
nchHW=input('Enter number of hot wire sensor channel (as vector): ');
% read hot wire raw data
fp=fopen(strcat(path,file),'r');
for n=1:nblock
a = readDataBlock(fp,nchannel);
t{n}=a(1,:)';T{n}=30*a(nchT,:)';E{n}=a(nchHW,:)';
end
fclose(fp);
% convert hot wire raw data to velocity in probe coordinate system
[cfile,cpath]=uigetfile('*.mat','Select hot wire calibration file');
load(strcat(cpath,cfile));
Tw=Tref*ones(size(Tcr20))+(R*ones(size(Tcr20)))./(Tcr20./(ones(size(Tcr20))...
+Tcr20*(Tref-20)));
ct=input(['Choose calibration type:\n 1 = spline interpolation\n...
  2 = spline interp.+ kings law\n 3 = kings law\n...
   4 = polynom of order ' num2str(np) '\n user input: ']);
nfft=input('Enter time segment length for fourier transform (as number of samples): ');
fS=input('Enter sampling frequency [Hz]: ');
if length(nchHW)==2
    k2=input('Enter yaw coefficients k^2 (as vector): ');
elseif length(nchHW)==3
    k2=input('Enter yaw coefficients k^2 (as vector): ');
    h2=input('Enter pitch coefficients h^2 (as vector): ');
end
rot=input('Do you want to rotate the hot wire velocities? (1=yes, 0=no) : ');
if rot==1
    ang=input('Enter rotation angle in degrees\n (as vector for triple wire,...
     first angle about x-axis, last about z-axis): ');
end
ppt=input('Save spectral plots as PowerPoint (1) or not at all (0) : ');
if ppt==1
    pptfile=input('Enter name of power point file: ','s');
end
for nb=1:nblock
    disp(['Converting raw data of block no. ' num2str(nb)]);
```

```
    Uc{nb} = HWE2Vb(E{nb},T{nb},Ecalc,Ucal,Tref,Tw,m,length(nchHW),CalCo,ne,CalPol,np,ct);
    if length(nchHW)==1
        V{nb} = Ucal2Vprobe(Uc{nb},length(nchHW));
    elseif length(nchHW)==2
        V{nb} = Ucal2Vprobe(Uc{nb},length(nchHW),k2);
    elseif length(nchHW)==3
        V{nb} = Ucal2Vprobe(Uc{nb},length(nchHW),k2,h2);
    end
    if rot==1
        V{nb} = rotHWvel(V{nb},ang,length(nchHW));
    end
    Vm{nb} = mean(V{nb});
    Vv{nb} = var(V{nb});
    [Ti{nb} aniso{nb}] = TurbInt(Vm{nb},Vv{nb},length(nchHW));
    for n=1:length(nchHW)
        [PSDV{nb}(:,n),f{nb}(:,n)] = pwelch((V{nb}(:,n)-Vm{nb}(n)),nfft,(nfft/2),nfft,fS);
    end
    figure(nb);clear leg;
    for n=1:length(nchHW)
        loglog(f{nb}(:,n),PSDV{nb}(:,n),symbols{n});hold on;
        leg{n}=['vel. comp. no. ' num2str(n)];
    end
    xlabel('f [Hz]');ylabel('PSD [m^2s^{-2}Hz^{-1}]');
    xlim([1 1e4]);
    legend(leg,'Location','Best');
    hold off;
    if ppt==1
        saveppt2(strcat(pptfile,'.ppt'));
    end
end
savepd=input('Do you want to save the processed data? (1=yes, 0=no) : ');
if savepd
    savename=input('Enter name for saving processed data: ','s');
    save(strcat(savename,'.mat'),'V','Vm','Vv','PSDV','f','Ti','aniso');
end
```

The function *Ucal2Vprobe.m*:

```
function V = Ucal2Vprobe(Uc,nHW,k2,h2)
% Ucal2Vprobe Converts calibration velocity into velocity in probe
% coordinate system
%   Uc is the calibration velocity
%   nHW is the number of wires
%   k and h are sensitivity factors of the probe
if nHW==1
    V=Uc;
elseif nHW==2
    MT=[(1+k2(1))*k2(2) -(1+k2(1));-(1+k2(2)) (1+k2(2))*k2(1)]/(2*(k2(1)*k2(2)-1));
    U=sqrt(Uc.^2*MT); % velocity in wire coordinate system
    R=[1 1;1 -1]/sqrt(2);
    V=U*R; % velocities in probe coordinate system
elseif nHW==3
    det=1+h2(1)*h2(2)*h2(3)-h2(3)*k2(1)-h2(1)*k2(2)-h2(2)*k2(3)+k2(1)*k2(2)*k2(3);
    MI=[(-h2(3)+k2(2)*k2(3)) (h2(1)*h2(3)-k2(3)) (1-h2(1)*k2(2));...
        (1-h2(2)*k2(3)) (-h2(1)+k2(1)*k2(3)) (h2(1)*h2(2)-k2(1));...
```

```
        (h2(2)*h2(3)-k2(2)) (1-h2(3)*k2(1)) (-h2(2)+k2(1)*k2(2))]/det;
    CM=diag([(1+k2(1)+h2(1)) (1+k2(2)+h2(2)) (1+k2(3)+h2(3))]);
    MT=(MI*CM/3)';
    U=sqrt(Uc.^2*MT); % velocity in wire coordinate system
    R=[1/sqrt(3) 1/sqrt(3) 1/sqrt(3); -1/sqrt(2) 1/sqrt(2) 0;...
        -1/sqrt(6) -1/sqrt(6) 2/sqrt(6)];
    V=U*R';
end

end
```

The function *rotHWvel.m*:

```
function [Vr] = rotHWvel(V,ang,nhw)
% rotHWvel rotates hot wire velocities
%   rotates velocities about the origin
%   the rotation angle has to be in degrees
%   positive rotation angle: counterclockwise rotation
%   3D rotation: ang has to be a vector, ang(1) is around x-axis,..., ang(3)
%   around z-axis; the order of rations around axes is: x, y, z
ang=ang*pi/180;
if nhw==2
    D=[cos(ang) -sin(ang);sin(ang) cos(ang)];
    Vr=V*D';
elseif nhw==3
    Dx=[1 0 0;0 cos(ang(1)) -sin(ang(1));0 sin(ang(1)) cos(ang(1))];
    Dy=[cos(ang(2)) 0 sin(ang(2));0 1 0;-sin(ang(2)) 0 cos(ang(2))];
    Dz=[cos(ang(3)) -sin(ang(3)) 0;sin(ang(3)) cos(ang(3)) 0;0 0 1];
    D=Dz*Dy*Dx;
    Vr=V*D';
end

end
```

The function *TurbInt.m*:

```
function [Ti aniso] = TurbInt(Vm,Vv,nhw)
% TurbInt calculates the turbulence intensity and the ratio of the
% variances of different velocity components
Um=0;
Uv=0;
for i=1:nhw
    Um=Um+Vm(i)^2;
    Uv=Uv+Vv(i);
    aniso(i)=Vv(i)/Vv(1);
end
Ti=sqrt(Uv/(nhw*Um));
end
```

C Correlation Function

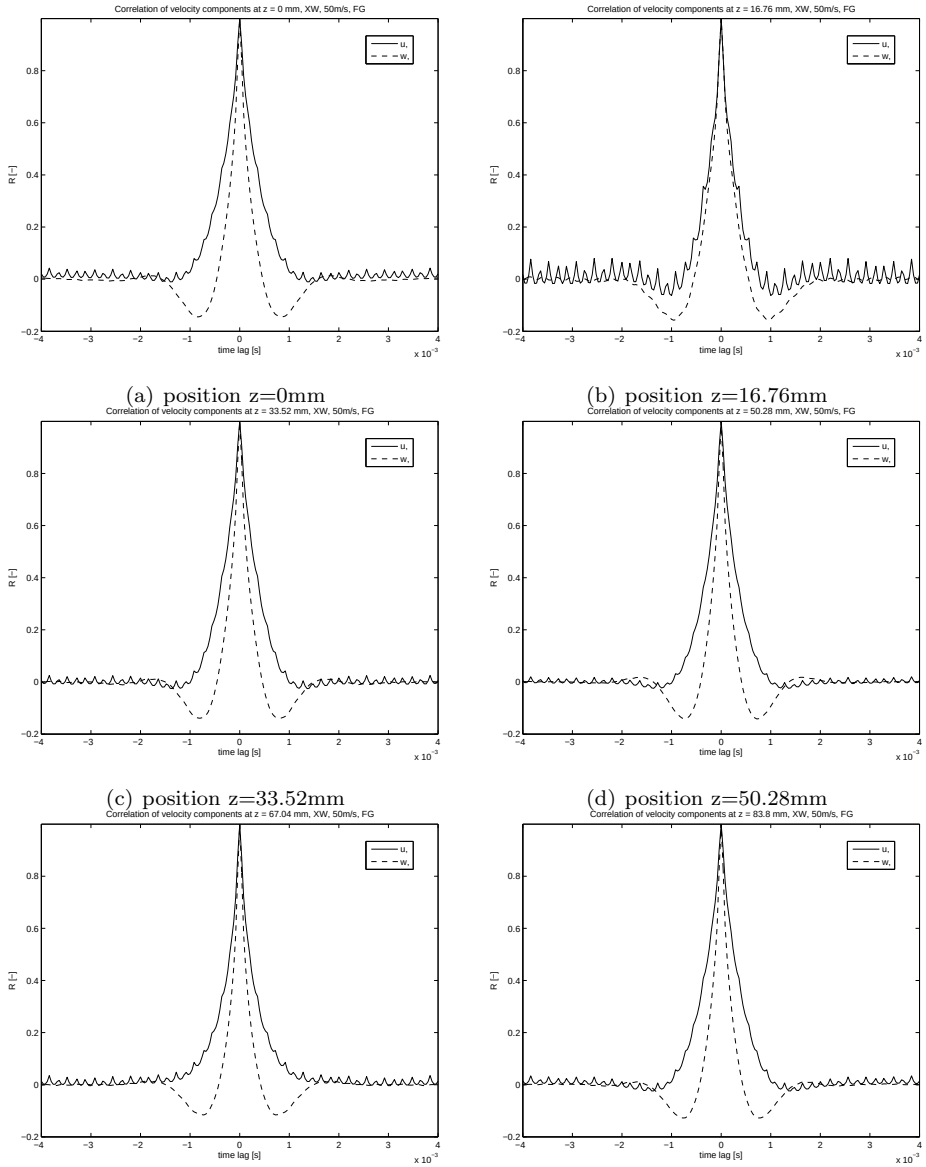

(a) position z=0mm

(b) position z=16.76mm

(c) position z=33.52mm

(d) position z=50.28mm

(e) position z=67.04mm

(f) position z=83.8mm

Figure 17. Correlation function for FG, Flow Speed 50m/s

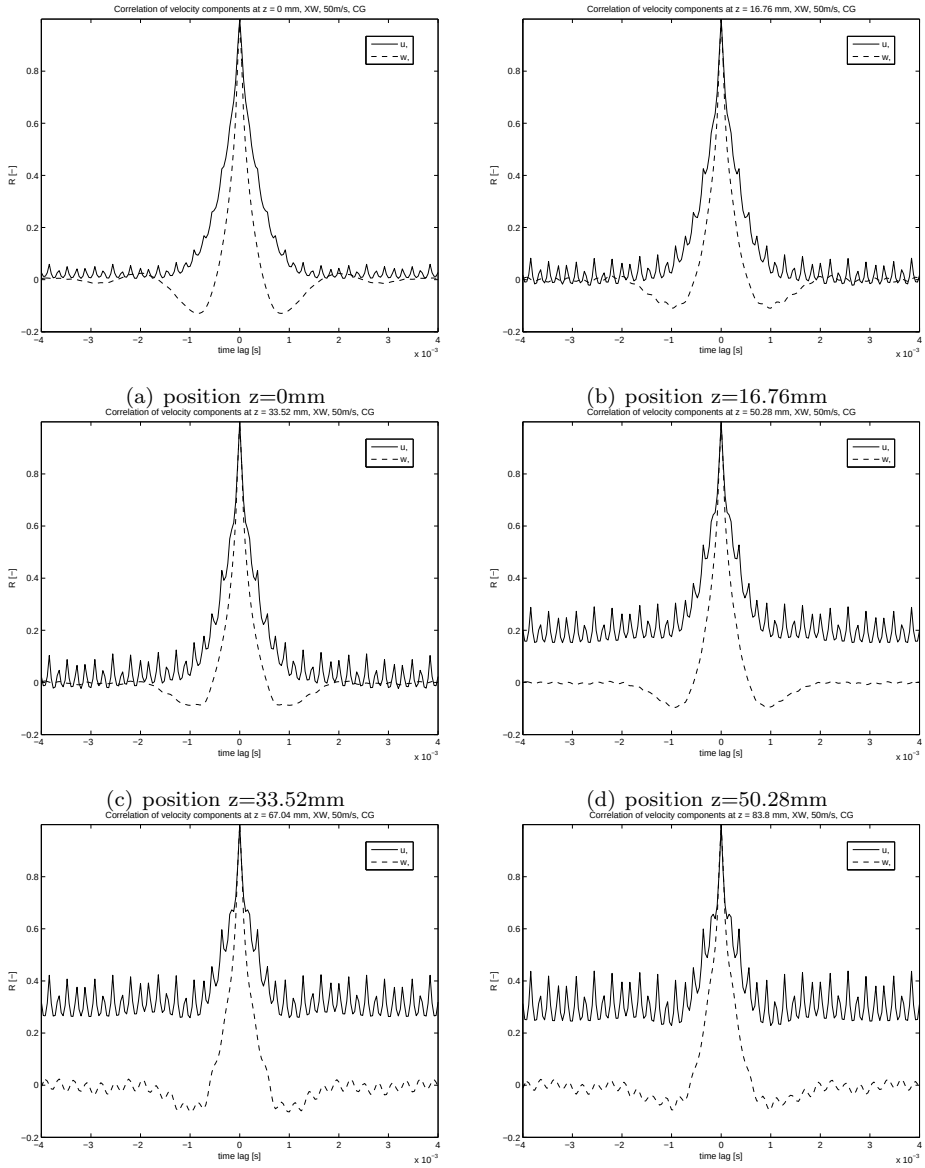

(a) position z=0mm

(b) position z=16.76mm

(c) position z=33.52mm

(d) position z=50.28mm

(e) position z=67.04mm

(f) position z=83.8mm

Figure 18. Correlation function for CG, Flow Speed 50m/s

DTU Wind Energy
Technical University of Denmark

Frederiksborgvej 399
4000 Roskilde
Denmark
Phone +45 4677 5024

www.vindenergi.dtu.dk